Colloidal nanoparticles trapped by liquid-crystal defect lines: A lattice Monte Carlo simulation

Regina Jose,[1,2] Gregor Skačej,[1,3] V. S. S. Sastry,[2] and Slobodan Žumer[1,3]
[1]*Faculty of Mathematics and Physics, University of Ljubljana, Jadranska 19, SI-1000 Ljubljana, Slovenia*
[2]*School of Physics, University of Hyderabad, Hyderabad 500046, Telangana, India*
[3]*NAMASTE Center of Excellence, Jamova 39, SI-1000 Ljubljana, Slovenia*
(Received 9 April 2014; published 8 September 2014)

Lattice-based Monte Carlo simulations are performed to study a confined liquid crystal system with a topological disclination line entangling a colloidal nanoparticle. In our microscopic study the disclination line is stretched by moving the colloid, as in laser tweezing experiments, which results in a restoring force attempting to minimize the disclination length. From constant-force simulations we extract the corresponding disclination line tension, estimated as ∼50 pN, and observe its decrease with increasing temperature.

DOI: 10.1103/PhysRevE.90.032503 PACS number(s): 61.30.Cz, 61.30.Jf, 47.57.J−

I. INTRODUCTION

Curvature elasticity-mediated interactions in confined nematic liquid crystals (LCs) have turned out to be a powerful tool for colloidal particle assembly both in two- and three-dimensional systems [1–4]. This mechanism is typically externally assisted by the use of laser tweezers allowing for a direct manipulation of colloidal particles in a refractive index-mismatched nematic medium [5,6]. The resulting colloidal crystals show great potential for use in various photonic applications [7]. A most relevant aspect in colloidal crystal assembly is the interaction of colloidal particles with nematic topological defect lines (disclinations): colloidal particles are known to be attracted towards disclinations if they are well within the influence of the corresponding distortion field [8–10]. Another important feature is the response of disclination-trapped particles to the application of an external force as provided in an experiment, e.g., through a laser tweezer in a disclination line tension measurement [5,11]. Moreover, when a colloidal particle is moved, this affects the surrounding nematic medium, including the disclination lines [4,12].

Here we present a simple microscopic lattice Monte Carlo (MC) simulation study of a small spherical colloidal nanoparticle trapped by a nematic disclination line, with a typical particle size around or even below 100 nm [13–15]. While there have been a number of experimental investigations in such systems, microscopic simulation studies are still rare. We focus on the particle force-displacement behavior when an external (e.g., laser tweezer) force is applied in an attempt to move the particle. To provide a controlled disclination line environment, a nematic liquid crystal sample confined to a prismatic nanochannel is considered. Nanochannel-confined colloidal particles have been studied in the past using phenomenological simulations [16], while our approach here is more microscopic and based on simple pairwise interactions. Recently, off-lattice molecular simulations have also been used to study small nanoparticles in LCs, focusing on particle diffusivity and interaction, gel formation, and particle positioning inside LC droplets [17–19].

II. MODEL, GEOMETRY, AND METHOD

Our approach is based on the Lebwohl-Lasher (LL) lattice model [20,21], where elongated LC molecules are represented by a system of freely rotating unit vectors (spins) $\mathbf{u}_i$ arranged into a simple cubic lattice of spacing a. The colloidal particle, as well as the confining nanochannel walls, are carved from the cubic lattice, with the corresponding interfacial spin orientations fixed according to the desired boundary conditions (anchoring). The total interaction energy is given by $U = -\epsilon \sum_{\langle ij \rangle} [3(\mathbf{u}_i \cdot \mathbf{u}_j)^2 - 1]/2$, where the sum is taken over nearest-neighbor lattice sites i and j, while $\epsilon > 0$ is the orientational interaction strength promoting parallel spin alignment. The nematic-nematic, nematic-colloidal particle, and nematic-wall interaction strengths are assumed equal, which implies strong surface anchoring with an extrapolation length [23] approaching $\sim a$. Temperature T is represented in reduced units as $T^* = k_B T/\epsilon$, with bulk nematic-isotropic (NI) transition occurring at $T^*_{\mathrm{NI}} \sim 1.1232$ [21].

The simulation box is simple cubic and periodic along the z direction, accommodating a prismatic nanochannel. The channel is directed along z and has a length $h = 100a$; its lateral (xy) cross section is an equilateral triangle of side length $l = 200a$. This leaves more than 1.73×10^6 lattice sites inside the channel, actively taking part in the simulation and constituting the bulk of our nematic medium (see Fig. 1). Bounding sites along the nanochannel surface are anchored planarly within the xy plane so as to create a stable disclination line of strength $m = -1/2$, running along the channel symmetry axis z. Through such boundary conditions we have explicitly avoided less stable integer-strength disclinations characterized by a higher free-energy cost per unit length $F_d \propto m^2$ that, in addition, are also prone to escape along z [23,24].

A spherical colloidal particle with strong homeotropic (normal) surface anchoring and $5a$ radius is fixed at the channel symmetry axis, serving to pin the edges of the disclination. Another similar colloidal particle with $10a$ radius is initially placed at the midpoint of the nanochannel axis, i.e., $h/2 = 50a$ away from the pinning particle (Fig. 1). In our study, we focus on the interplay between the disclination line and this second colloidal particle (which is either kept fixed in position or mobile), taking its initial position (channel center) as the origin of our reference frame $\mathbf{r}_c = (0,0,0)$ and denoting its instantaneous position (with respect to the MC "time") with $\mathbf{r}_c = a(x_c, y_c, z_c)$. The inclusion of the movable particle makes an otherwise straight disclination line loop around it, entangling it in the process. In this way a particle inclusion and a disclination are mutually affined, and hence the disclination

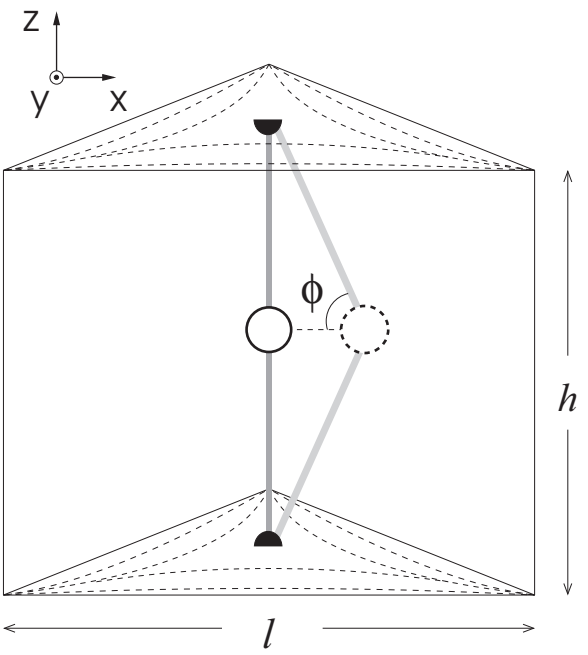

FIG. 1. Schematic of the simulated nanochannel: dashed lines at the top and bottom surfaces represent the director field. The colloidal particle under study (white) is at the center and the smaller pinning particle (black) is at the channel top and bottom (note the periodic boundary conditions). The disclination (dark gray line) runs along the channel axis. The particle in a shifted position along with the stretched disclination is also shown in lighter shades. The defect structure around the particles is not explicitly shown.

can be stretched by pulling the particle away from the channel center. Excess pulling can cause the disclination to detach from the particle and relax by retracing to its initial unstretched configuration.

We explore the behavior of our model system using Markov chain MC simulations. The underlying phase space consists of nematic spin orientations $\mathbf{u}_i$ and positions, as well as of the moving particle coordinates $\mathbf{r}_c$. In simulations where the particle is fixed, the MC evolution affects exclusively the nematic spin orientations and follows the standard Metropolis procedure [21,25,26]. Here single-spin reorientational trial moves are generated using the Barker-Watts technique [27] and are accepted with a probability $\min[1, \exp(-\Delta U/k_BT)]$, where ΔU is the corresponding interaction energy change. The acceptance ratio is kept close to 0.5 by dynamically adjusting the spin reorientation amplitude. A standard MC sweep is defined as an attempted reorientation of all nematic spins.

In simulations where the particle is mobile, on the other hand, composite particle moves are performed in addition: first, the particle is shifted randomly by a lattice unit and the nematic spins annihilated in this way are recreated in the newly established void on the other side of the particle. The recreated spins are given orientations compliant with the particle-imposed boundary conditions, which is refined by 1000 relaxation sweeps (see below) involving additional LC spins in particle vicinity. The acceptance or otherwise of this composite particle move is, as above, guided by the Metropolis criterion, ΔU here denoting the total interaction energy difference before and after the attempted composite move. The relaxation sweeps performed prior to the acceptance or rejection are essential to facilitate the insertion of the displaced particle equilibrated with respect to the existing nematic director field. They are carried out according to the Metropolis scheme used in fixed-particle runs, but involve, for computational time and trial move acceptance reasons, only spins within a thin shell of $3a$ thickness surrounding the particle. (In any case the immediate reorienting influence of the moving particle is expected to be stronger in its vicinity.) After every attempted composite move, further 1000 standard MC sweeps are performed without moving the particle, to relax the entire director field, and this sets a unit of MC simulation "time" t_c. This algorithm is intended to reflect and account for the difference between the slower translational time scale associated with the larger and massive particle, compared to the faster reorientations of the LC spins constituting the nematic medium.

Note that, once the system has reached equilibrium and detailed balance is obeyed, the above Metropolis acceptance criterion generates the desired (canonical) distribution in phase space only if a given trial move and its reverse are attempted with equal probabilities [26]. While this is certainly the case for individual spin reorientations [27], it is much less obvious for our composite moves where the probability of attempting a particle displacement (together with a specific orientational configuration of the surrounding nematic spins) may, at least in principle, depend on particle position. This arises due to the instinctual inadequacy of the procedure to sample the available phase space (for the geometry considered here) in a perfectly unbiased way. In the cases considered in this work, i.e., for small particle displacements along the x axis far enough from the confining walls, we expect this dependence to be negligible; therefore, forward and reverse move attempts should be equally probable and eventually result in the canonical asymptotic distribution.

In analogy with tweezing experiments wherein an adequately intense laser is used to pull the particle, in our simulations an external constant force $\mathbf{F}$ is applied. In such a case the Metropolis criterion for acceptance probability of the particle move is modified to $\min\{1, \exp[-\Delta(U - \mathbf{F}\cdot\mathbf{r}_c)/k_BT]\}$ [26,28]. In the following, external force is given in dimensionless units $F^* = |\mathbf{F}|a/\epsilon$. Taking $\epsilon \sim 0.023$ eV, which yields a bulk NI transition at room temperature [21], and $a \sim 1$ nm, which roughly assumes one spin to represent a single LC molecule [20,29], a unit of F^* corresponds to $\sim$3.7 pN.

To identify and visualize topological defects, Westin metrics are calculated for each lattice site i from the eigenvalues $\lambda_1^i \geqslant \lambda_2^i \geqslant \lambda_3^i$ of the averaged local ordering matrix $\langle \mathbf{u}_i \otimes \mathbf{u}_i \rangle$: $c_l^i = \lambda_1^i - \lambda_2^i$, $c_p^i = 2(\lambda_2^i - \lambda_3^i)$, and $c_s^i = 3\lambda_3^i$, with $0 \leqslant c_l^i, c_p^i, c_s^i \leqslant 1$ [30]. c_l^i, c_p^i, and c_s^i approaching $\sim$1 correspond to prominent uniaxial, planar, and isotropic orderings, respectively. Since the defect core is characterized by depressed uniaxial order, compared to the rest of the medium, it can be visualized by constructing isosurfaces of c_l^i obtained from the $\mathbf{u}_i$ field, at an appropriately chosen (temperature-dependent) threshold. The averaging of the local ordering matrix is performed over the six nearest-neighbor lattice sites, apart from the test site, from an instantaneous

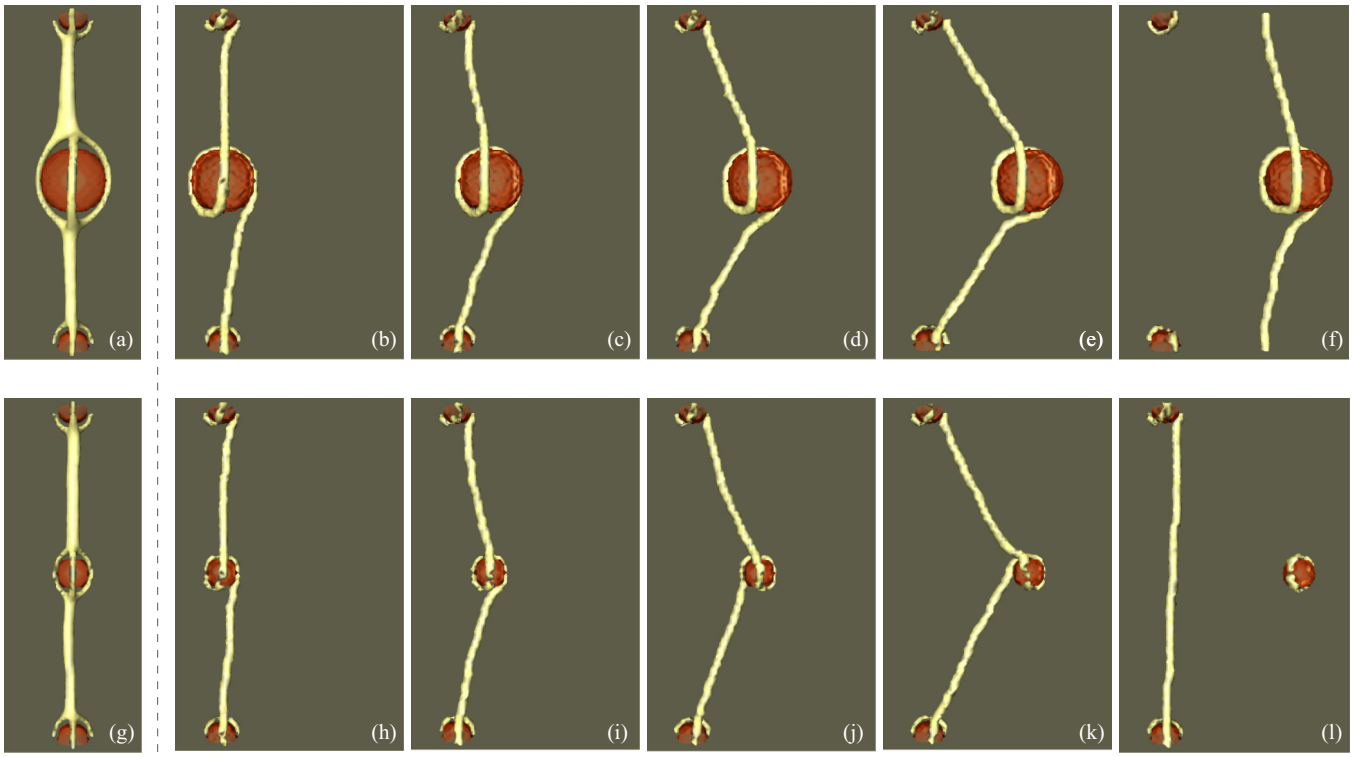

FIG. 2. (Color online) Top row shows defect structures (yellow) entangling a colloidal particle (red) of radius $10a$, obtained with (a) the particle positioned at origin for $T^* = 1.0$, averaged over MC sweeps (MDS) and, (b)–(f) with $x_c = 0$, 10, 20, 30, and 40 for $T^* = 0.1$ from an equilibrated instantaneous configuration (IDS). Bottom row displays similar structures for a smaller particle of radius $5a$. Disclinations are visualized as c_l^i isosurfaces for a threshold of 0.85 and 0.28 at the lower and higher temperatures, respectively. (The corresponding bulk values are approximately 0.98 and 0.6.) Note the apparent variation in the looping of disclination line around the colloid, and the thickness of the line away from the particle, at both temperatures. See text for a more detailed description and Supplemental Material [22] for the movies. The small particle seen at the top and bottom in each plate serves to pin the disclination line.

configuration or, alternatively, over a large number of MC sweeps. A so-called "instantaneous defect structure" (IDS) is obtained in the first case, and a "mean defect structure" (MDS) in the second. In our figures, IDS and MDS are typically shown for lower and higher values of T^*, respectively.

Along the length of simulation nanochannel, the nematic director field surrounding the disclination line is nearly identical except near the particle, and hence translations of the particle along the z axis are energetically largely inconsequential. In our simulations we set $z_c = 0$, and translation moves of the particle are restricted along the x axis, without loss of generality. This is to scale down the computational time to manageable limits, given the three-dimensional sample space within the channel. Nevertheless, it still helps us to capture the essential qualitative behavior of the system studied.

III. RESULTS AND DISCUSSION

A. Equilibrium defect structures with fixed particle positions

Initially we look at the equilibrium defect structures in the system as a function of colloidal particle position, along the x axis. The particle, initially positioned at the origin, $x_c = 0$, is shifted off-center step-by-step to the adjacent sites, after equilibrating the medium with 2×10^5 MC sweeps during each step. Figure 2(a) shows the defect structure obtained by averaging the local-ordering matrix over the latter 10^5 MC sweeps with particle at $x_c = 0$ and $T^* = 1.0$. Figures 2(b) to 2(f) show the IDS structure sequence obtained after each translational step at $T^* = 0.1$. It may be noted that during the equilibration sweeps in each of these steps the particle position remains fixed. As the particle is shifted away from center, the disclination line stretches itself, still entangling the particle, up to a threshold distance above which a detachment occurs. This threshold is observed at $x_c \sim 35$ for $T^* = 0.1$, and occurs at a smaller value of x_c at higher temperatures. For comparison, similar data for a smaller particle of radius $5a$ are shown in the bottom row of Fig. 2.

At $T^* = 1.0$ the defect structure appears to have a three-fold symmetry wherein it forks into three branches around the particle and then rejoins to a single disclination. Qualitatively similar structures are also observed in our preliminary off-lattice simulations based on the soft-core Gay-Berne potential [31], performed at a similar temperature rather close to the NI transition. In the present lattice simulations this structure apparently gets modified as the temperature is lowered. This can be attributed to reduced defect line bending near the particle in accordance with larger line tensions under these conditions. Note that sometimes transformations between different entangling structures occur also during the course of simulations at fixed external parameter values [for instance,

see the difference between the entangling of the displaced colloid by the disclination line in Figs. 2(i) and 2(j)]. It is seen that when the large ($10a$ radius) moving particle is considered, it is the disclination that detaches from the pinning particle, on shifting the particle far away from the center. For the small ($5a$ radius) particle, the opposite is true: the disclination detaches from the moving particle instead, relaxing back to the center, while leaving the moving particle with a Saturn ring defect [32]. This can be attributed to a more pronounced anchoring effect by the larger particle at this temperature. Another effect of temperature is on the fluctuations of the disclination line itself. A manifestation of its spatial fluctuations over MC "time" is seen as an increase in the disclination line thickness in regions far away from the particles as in Figs. 2(a) and 2(g), at $T^* = 1.0$. A qualitative view of these fluctuations is observed in the movies (see the Supplemental Material [22]) showing a series of defect structures obtained at $T^* = 0.1$ and 1.0, as the particle position is shifted away from the channel center. For $T^* = 1.0$, a superimposed second isosurface at a higher threshold of $c_l^i = 0.53$ enveloping the one with a lower c_l^i alludes to the fact that the defect structures formed for different system parameters in our simulations are all qualitatively similar.

B. Unstretching of disclination line with mobile particle

Now we extend our simulations by allowing colloidal particle translation as the system evolves during MC "time" t_c to explore the ability of a stretched disclination to move an entangled particle. In this case we take an initial configuration of the system where the particle is at $x_c > 0$, entangled by a stretched disclination. In an experiment this is achieved by pulling the disclination affined either to an isotropic laser-created region, or to a particle tweezed by a laser, and then withdrawing the laser intensity. This corresponds to a state similar to that depicted in Fig. 2(d) where the particle is at $x_c = 20$ units away from the origin. The trail of the moving particle is monitored over t_c and is shown in Fig. 3. In all cases the particle is found to be drawn, approximately, back to the origin at $x_c \sim 0$, adducing the presence of a restoring force which drives the relaxation of the disclination to its equilibrium. This indeed should be expected since a shorter disclination corresponds to lesser volume occupied by the defect region, thereby reducing the total free energy. Note that in some cases the equilibrated particle position is slightly off-centered, with typically slightly negative equilibrium x_c values; this is attributed to the asymmetric particle entanglement (see Fig. 2). Note also that very large fluctuations in the particle position occur at higher temperatures, and so most of our simulations are performed at relatively low T^* to facilitate the analysis.

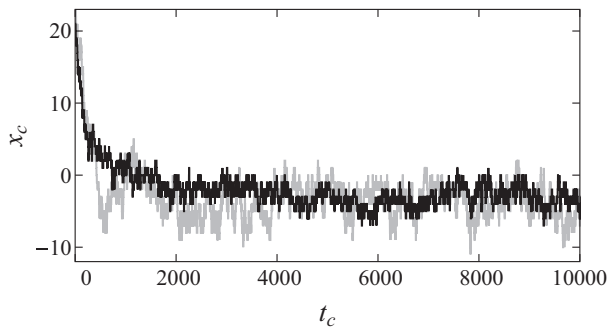

FIG. 3. Trail of the particle as the system evolves from an initially stretched entangled disclination with particle at $x_c = 20$, along x at $T^* = 0.1$ (black) and 0.15 (gray).

C. Constant-force simulations with mobile particle

Next we perform constant-force simulations wherein a constant force F^* is applied to the particle initially positioned at the origin. The force is applied along the positive x axis and, for simplicity, the particle motion is also restricted along the same axis. Initially, the force shifts the particle away from the origin and after a transient time this distance is seen to equilibrate over a mean value, when the system arrives at a nearly steady state. This occurs when the restoring force (manifested through disclination line tension) balances with the external force F^*. Larger F^* values result in an equilibration farther from the origin. Beyond a threshold value of force, a detachment occurs. It is ensured that such simulations are discarded by monitoring the defect structures at regular intervals as the simulation proceeds. We observe in all cases that the particle position x_c equilibrates within first $2000t_c$; then its average is determined over the next $8000t_c$. These simulations are carried out at various temperatures.

The dependence of average equilibrated distance $\langle x_c \rangle$ on the applied force F^* at different temperatures is shown in Fig. 4(a). The reasonably good linear fits (with Pearson's correlation coefficients $\geqslant 0.95$) suggest Hookean behavior, permitting the comparison of disclination with an elastic string. (Again, at zero force, slightly negative $\langle x_c \rangle$ are observed, which is consistent with our above reasoning.) Slopes obtained from the fits are inverse values of Hookean force constants k^*, with their temperature dependence shown in Fig. 4(b). These values translate to real units as $\epsilon k^*/a^2$ and are, for the a and ϵ estimates given in Sec. II, in the range of $\sim 1.5 \times 10^{-3}$ N/m. In the temperature range considered here, typical line tension values just before detachment at $x_c \sim 20$ ($\tan\phi = h/2x_c \sim 2.5$, see Fig. 1) and $F^* \sim 10$ are estimated as $F_d = F^*\epsilon/2a\cos\phi \sim 50$ pN, which agrees well with experiments yielding values between 20 and 120 pN [5,11,33]. Note that this estimate of F_d is sensitive to the choice of the lattice spacing parameter value a. (Sometimes, a nematic spin in the LL model is taken to represent a close-packed cluster of up to $\sim 10^2$ molecules rather than a single molecule [34], yielding a somewhat larger a and, in turn, a smaller F_d.) Moreover, like in experiments [33], our data displayed in Fig. 4(b) suggest a decrease of the line tension with increasing temperature. This also agrees with the phenomenological prediction $F_d \propto K$, where K, the Frank elastic constant of the nematic LC, decreases with increasing temperature [23,24]. Finally, F_d is a liquid-crystalline material property and should be independent from the specific geometrical setup of our simulated experiment, i.e., nanochannel size parameters h and l, as well as the external force pulling direction.

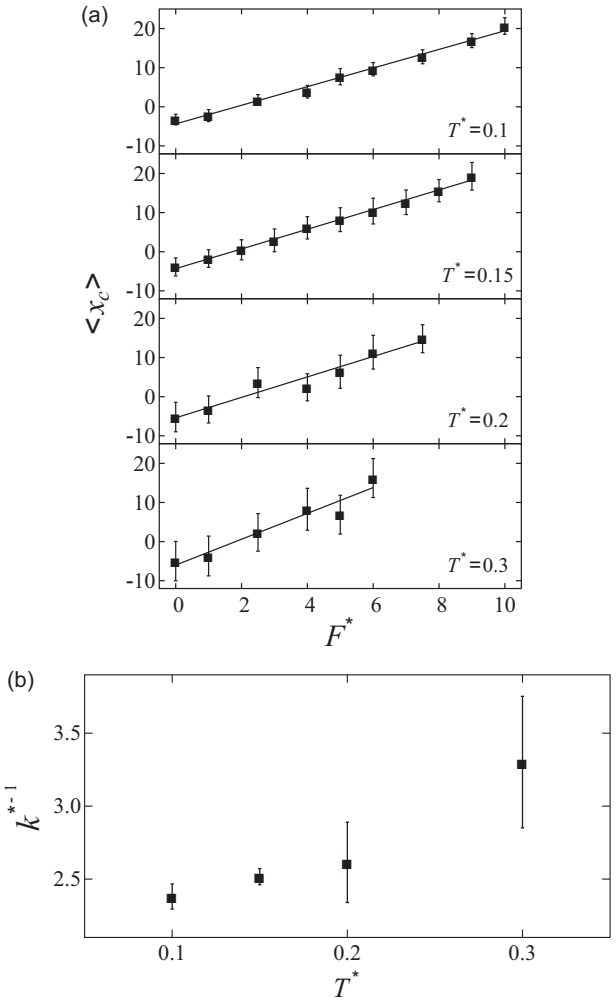

FIG. 4. (a) Equilibrium colloidal particle position versus applied force for different temperatures. Straight lines represent Hookean linear fits. (b) Temperature dependence of the force constant inverse $1/k^*$.

IV. CONCLUSION

A simple microscopic spin model is employed to study a nematic liquid-crystalline system containing a spherical particle entangled by a disclination line, using lattice-based MC simulations. The conventional single-spin-flip Markov chain MC procedure is adapted to incorporate the multiscales entering into the problem via the relatively slow translational motion of a larger particle in equilibrium with the surrounding liquid-crystalline medium. It is seen that our simulations qualitatively capture the physical behavior of a real system, including an estimate for the disclination line tension in the range of ∼50 pN and its decrease with increasing temperature. Simulation methods adopted here enable us to study a reasonably large system and allow us, at the same time, to look into the detailed nanoscale behavior. Currently, this would have been less practicable using an off-lattice model, coarse-grained or atomistic, for reasons of unacceptable computational cost. On the other hand, we also deliberately avoid continuum-based phenomenological approaches due to the constraints in the lower limit of the length scales they can probe into.

ACKNOWLEDGMENTS

Support from the European Union (EC ITN Marie Curie research network HIERARCHY, NAMASTE Center of Excellence) and from the Slovenian Research Agency (P1-0099) is gratefully acknowledged. The authors also acknowledge helpful discussions with K. P. N. Murthy on certain finer points of Monte Carlo methods, and T. Porenta on the phenomenological aspects of the problem. R.J. thanks the University of Hyderabad and Council of Scientific and Industrial Research (CSIR), India for granting the leave facilitating the visit to Slovenia. Simulations were performed in the computing clusters at the Center for Modeling Simulation and Design at the University of Hyderabad and at the Faculty of Mathematics and Physics, University of Ljubljana.

[1] I. Muševič, M. Škarabot, U. Tkalec, M. Ravnik, and S. Žumer, Science **313**, 954 (2006).
[2] A. Nych, U. Ognysta, M. Škarabot, M. Ravnik, S. Žumer, and I. Muševič, Nat. Commun. **4**, 1489 (2013).
[3] M. Ravnik, G. P. Alexander, J. M. Yeomans, and S. Žumer, Proc. Natl. Acad. Sci. **108**, 5188 (2011).
[4] T. Araki, F. Serra, and H. Tanaka, Soft Matter **9**, 8107 (2013).
[5] I. I. Smalyukh, A. N. Kuzmin, A. V. Kachynski, P. N. Prasad, and O. D. Lavrentovich, Appl. Phys. Lett. **86**, 021913 (2005).
[6] M. Škarabot, M. Ravnik, D. Babić, N. Osterman, I. Poberaj, S. Žumer, I. Muševič, A. Nych, U. Ognysta, and V. Nazarenko, Phys. Rev. E **73**, 021705 (2006).
[7] S. Žumer, I. Muševič, M. Ravnik, M. Škarabot, I. Poberaj, D. Babić, and U. Tkalec, Proc. SPIE **6911**, 69110C (2008).
[8] D. Pires, J.-B. Fleury, and Y. Galerne, Phys. Rev. Lett. **98**, 247801 (2007).
[9] J.-B. Fleury, D. Pires, and Y. Galerne, Phys. Rev. Lett. **103**, 267801 (2009).
[10] P. Kossyrev, M. Ravnik, and S. Žumer, Phys. Rev. Lett. **96**, 048301 (2006).
[11] N. Osterman, J. Kotar, E. M. Terentjev, and P. Cicuta, Phys. Rev. E **81**, 061701 (2010).
[12] T. Araki and H. Tanaka, J. Phys.: Condens. Matter **18**, L193 (2006).
[13] A. V. Ryzhkova and I. Muševič, Phys. Rev. E **87**, 032501 (2013).
[14] J. Milette, V. Toader, E. R. Soule, R. B. Lennox, A. D. Rey, and L. Reven, Langmuir **29**, 1258 (2013).
[15] G. M. Koenig, Jr., J. J. de Pablo, and N. L. Abbott, Langmuir **25**, 13318 (2009).
[16] F. R. Hung, B. T. Gettelfinger, G. M. Koenig, Jr., N. L. Abbott, and J. J. de Pablo, J. Chem. Phys. **127**, 124702 (2007).
[17] J. A. Moreno-Razo, E. J. Sambriski, G. M. Koenig, E. Díaz-Herrera, N. L. Abbott, and J. J. de Pablo, Soft Matter **7**, 6828 (2011).
[18] J. K. Whitmer, A. A. Joshi, T. F. Roberts, and J. J. de Pablo, J. Chem. Phys. **138**, 194903 (2013).

[19] J. K. Whitmer, X. Wang, F. Mondiot, D. S. Miller, N. L. Abbott, and J. J. de Pablo, Phys. Rev. Lett. **111**, 227801 (2013).
[20] P. A. Lebwohl and G. Lasher, Phys. Rev. A **6**, 426 (1972).
[21] U. Fabbri and C. Zannoni, Mol. Phys. **58**, 763 (1986).
[22] See Supplemental Material at http://link.aps.org/supplemental/10.1103/PhysRevE.90.032503 for a movie showing the evolution of defect structures as the particle position is shifted.
[23] P. G. de Gennes and J. Prost, *The Physics of Liquid Crystals* (Clarendon, Oxford, 1993).
[24] P. M. Chaikin and T. C. Lubensky, *Principles of Condensed Matter Physics* (Cambridge University Press, Cambridge, England, 1997).
[25] N. Metropolis, A. W. Rosenbluth, M. N. Rosenbluth, A. H. Teller, and E. Teller, J. Chem. Phys. **21**, 1087 (1953).
[26] D. Frenkel and Berend Smit, *Understanding Molecular Simulation: From Algorithms to Application* (Academic, San Diego, CA, 2002).
[27] J. A. Barker and R. O. Watts, Chem. Phys. Lett. **3**, 144 (1969).
[28] G. Raos and G. Allegra, J. Chem. Phys. **113**, 7554 (2000).
[29] C. W. Greeff and M. A. Lee, Phys. Rev. E **49**, 3225 (1994).
[30] A. C. Callan-Jones, R. A. Pelcovits, V. A. Slavin, S. Zhang, D. H. Laidlaw, and G. B. Loriot, Phys. Rev. E **74**, 061701 (2006).
[31] R. Berardi, C. Zannoni, J. Lintuvuori, and M. Wilson, J. Chem. Phys. **131**, 174107 (2009).
[32] E. M. Terentjev, Phys. Rev. E **51**, 1330 (1995).
[33] A. Mertelj and M. Čopič, Phys. Rev. E **69**, 021711 (2004).
[34] C. Chiccoli, P. Pasini, F. Semeria, E. Berggren, and C. Zannoni, Mol. Cryst. Liq. Cryst. **266**, 241 (1995).